

Copyright notice:

©2011 IEEE. Personal use of this material is permitted. However, permission to reprint/republish this material for advertising or promotional purposes or for creating new collective works for resale or redistribution to servers or lists, or to reuse any copyrighted component of this work in other works must be obtained from the IEEE.

Provision of Load Frequency Control by PHEVs, Controllable Loads, and a Cogeneration Unit

Matthias D. Galus, *Student Member, IEEE*, Stephan Koch, *Student Member, IEEE*, and Göran Andersson, *Fellow, IEEE*

Abstract—This paper presents a method for tracking a secondary frequency control (Load Frequency Control) signal by groups of plug-in hybrid electric vehicles (PHEVs), controllable thermal household appliances under a duty-cycle coordination scheme, and a decentralized combined-heat-and-power generation unit. The distribution of the control action on the participating units is performed by an aggregator utilizing a Model Predictive Control strategy which allows the inclusion of unit and grid constraints. In addition to the individual dynamic behavior, the varying availability of the units during the day is taken into account. The proposed methodology, easily extendable to larger networks, is evaluated on a four-bus system corresponding to a medium-voltage distribution grid and illustrates a possible operation mode of an aggregator in the power system.

Index Terms—Aggregators, cogeneration, electric appliances, Load Frequency Control (LFC), load management, plug-in hybrid electric vehicles (PHEVs), smart grids, vehicle to grid (V2G), virtual power plants.

I. INTRODUCTION

THE paradigm change toward a more sustainable electricity system is leading to an expansion of renewable generation and, hence, to a growing amount of fluctuating infeeds into transmission and distribution grids. High-accuracy forecasting techniques exist but they are not capable of completely avoiding infeed prediction errors. This tends to increase the active-power imbalances, which are always present in power systems, due to short-term load variations, load-prediction errors, and schedule changes. Therefore, a larger amount of control reserves is needed to balance supply and demand at all times. These are usually contracted by the Transmission System Operator (TSO) through ancillary-service markets [1].

Recently, the utilization of Demand Side Management (DSM) for such services has been shifting into focus [2]. DSM offers the potential to aggregate large numbers of flexible loads into substantial amounts of controllable power, potentially capable of replacing conventional control reserves. Household appliances with thermal inertia, such as refrigerators, freezers, and electric water heaters, could be utilized for DSM as they

imply a substantial energy-storage potential, which allows for a temporary reduction or increase of consumption. The distributed nature of these appliances needs efficient communication and proper standards, which are already partly in place [3]. Furthermore, the anticipated electrification of the individual vehicle fleet via electric vehicles (EVs) and plug-in hybrid EVs (PHEVs) [4] would result in an additional and complementary distributed storage. The vehicles are envisioned to not only impose load on the system while recharging but to also feed energy back into the grid while being in the so-called vehicle-to-grid (V2G) mode. This energy feedback is facilitated through recent and anticipated future advances in battery technology [5].

In order to ensure a well-coordinated utilization of the controllable resources, aggregators were proposed to cluster and manage large numbers of distributed energy resources. These may comprise both generation units and stationary loads [6], as well as large numbers of vehicles [7]. As to the latter case, substantial revenue potentials have been found for V2G services in different ancillary service markets in the U.S. [8] and in Europe [9]. However, the provision of such ancillary services may have a large impact on the providing entities. This impact must be confined within acceptable boundaries by the aggregator's control strategies in order to facilitate customer acceptance. In the case of thermal household appliances, a certain temperature band shall not be exceeded, while for vehicles, there may be restrictions imposed by a desired battery state of charge (SOC) for transportation purposes. Thus, the principal challenge of operation strategy design for ancillary services is constituted by the balance between the global control requirements from the grid side and the local impact on the individual customer.

This paper aims at contributing to the discussion on the integration of aggregators into power systems. Here, the aggregator uses a predictive-control approach, capable of observing input and state constraints, to follow a Load Frequency Control (LFC) signal. The thereby determined set points for the aggregated clusters, composed of a large PHEV fleet in V2G mode and large numbers of household appliances, consider the underlying physical-network state and the aggregate state information of the appliance populations. The set points applied to the clusters cause local reactions of selected individual units in order to deliver the control response. Complementary to studies showing the economic feasibility of an aggregator [7], [8] and the technical feasibility from the TSO's point of view, [10], [11], this paper shows the technical feasibility from a distribution system operator's (DSO's) point of view. The investigated approach considers crucial information exchange between the TSO, the DSO, and the aggregator.

Manuscript received April 30, 2010; revised August 17, 2010; accepted December 8, 2010. Date of publication January 20, 2011; date of current version August 30, 2011. This work was supported in part by the Swiss Federal Institute of Technology Zurich (ETH Zurich) under the ARTEMIS Project, focusing on the efficient plug-in hybrid electric vehicle integration into power systems, under Research Grant TH 2207-3, and in part by Swisselectric research under the Project, Local Load Management.

The authors are with the EEH-Power Systems Laboratory, Swiss Federal Institute of Technology (ETH) Zurich, 8092 Zurich, Switzerland (e-mail: galus@eeh.ee.ethz.ch; koch@eeh.ee.ethz.ch; andersson@eeh.ee.ethz.ch).

Digital Object Identifier 10.1109/TIE.2011.2107715

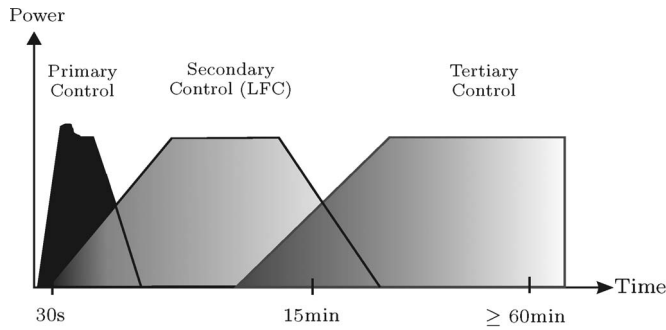


Fig. 1. Approximate time scales of frequency control-reserve activation and delivery in the Central Europe system (exact timing may vary).

First, a brief introduction to LFC is provided in Section II. Then, the system which is used for the study is described in Section III, including the individual and aggregated representations of the controlled entities. In Section IV, the control problem of the aggregator is formulated, and Section V presents numerical results. Finally, these are discussed in Section VI, and conclusions are drawn in Section VII.

II. LFC

In general, frequency control in power systems comprises primary, secondary, and tertiary control reserves contracted by the TSO.¹ The term LFC is used here as an equivalent to secondary control in accordance with the glossary contained in [12]. It is also referred to as Automatic Generation Control, although this term becomes somewhat inadequate once the utilization of controllable loads is considered.

This section presents a brief overview on frequency control in general, as well as the specific requirements for the provision of LFC relevant for the purpose of this paper.

A. General Aspects of Frequency Control

As illustrated in [13], the properties of control reserves can vary significantly from country to country, even within a common synchronous area. Therefore, the common guidelines for the Continental Europe system (ENTSO-E CE, former UCTE area) set forth in [12] (Policy P1 and Appendix A1: LFC and Performance) are used here as a basis. Usually, all three kinds of control reserves (primary, secondary, and tertiary) are tendered by the TSO in individually specified quantities for the respective control area, both as positive (generation increase or load decrease) and negative (generation decrease or load increase) reserves. Fig. 1 shows an overview of the activation and delivery times for the various control reserves. The necessary amounts are usually determined by probabilistic considerations [14] and largely depend on the size and generation portfolio of the control area.

Primary control reserves are activated by a decentralized proportional controller within the speed governors of generating units. In Continental Europe, the primary reserve has to be fully

¹This paper uses the operational terms defined by the European Network of Transmission System Operators for Electricity (ENTSO-E). The same service might be called differently in other power-system operation areas.

activated within 30 s and has to be sustained for a maximum of 15 min. The frequency droop has to be such that the full reserve is activated before a frequency deviation of 200 mHz occurs.

Secondary control reserves are activated by a proportional-integral (PI) controller usually operated by the TSO. These reserves are mainly used to relieve primary control, to bring the system frequency back to its nominal value, and to ensure the maintenance of the scheduled tie-line exchanges with other control areas. The secondary control signal transmitted by the TSO to the providing units in its control zone is dependent on the Areal Control Error (ACE), which should be controlled to zero. Equation (1) denotes the calculation of the ACE in Continental Europe, where P_{me} is the measured value of the total power exchange with other control zones, P_{se} is the scheduled power exchange with the other control zones, K_{ri} is the K -factor of the control area, f_m is the measured value, and f_t is the set value of the frequency

$$ACE = P_{me} - P_{se} + K_{ri}(f_m - f_t). \quad (1)$$

In principle, secondary-reserve capacity can be offered asymmetrically (meaning, a different scaling of positive and negative reserves), although this is used in very few countries.

Tertiary control is a manually activated reserve which is used to relieve the secondary control reserves. It must be fully activated usually after 15 min.

B. Requirements on Units Providing LFC

Generation units which shall be used for the provision of LFC are subject to specific requirements in order to ensure a guaranteed delivery of the control power demanded in real-time operation, as well as a good control performance. One major aspect is the accuracy of the LFC signal tracking, particularly the achievable gradients of power-generation changes. Reference [12] states that these requirements shall be adapted to the unit type because of individually different dynamic properties. More detailed requirements are usually set forth in the transmission code of the respective country. Standardized prequalification procedures may be used to determine and to certify the ability of a generation unit to provide LFC.

As an example, recent rules of the Swiss TSO [15], [16], which include a prequalification procedure, are considered here. Although the procedure is tailored for generation units at the current stage, it will be used in this paper for evaluating the proposed LFC approach. This is to show that no fundamental changes have to be introduced in the legislation when allowing the inclusion of controllable loads in the LFC systems.

The prequalification test mainly consists of a standardized power profile, shown here in Fig. 2, that has to be tracked by the unit in question. Certain tolerance bands are established within which a deviation from the power set point is permissible. The control signal $Y[\%]$ is shown as a percentage of the offered control band and has to be scaled according to the offered amount of reserves. Reference [15] states that this control band (difference between maximum and minimum power) should comprise at least 60% of the nominal output of a generation unit and must be greater than 10 MW. Only symmetrical bids

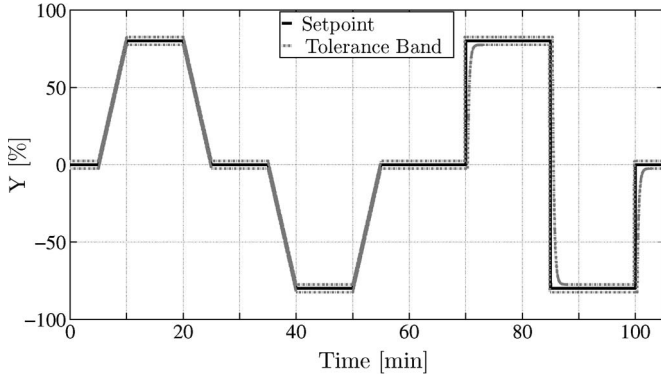


Fig. 2. Exemplary LFC prequalification-test profile based on [15].

for secondary reserves (equal amount of positive and negative control band) are currently permitted in Switzerland. This, however, is not a principal requirement.

The profile to be tracked, shown in Fig. 2, exhibits a number of set-point changes in ramp and step form over a total period of 105 min. In the second half of the curve, steps are imposed on the output power, which obviously cannot be followed with infinite accuracy by generation units which always have a constrained ramp rate. As a typical power plant set-point change behavior has a first-order characteristic, the tolerance band is delimited here by a first-order lag element. The time constant of this is calculated from the unit gradient specified in the transmission code. Here, as a worst case scenario, the highest gradient is chosen, which is 0.5% of the nominal power per second for hydropower plants. This is done to show that the considered load units, even under the most stringent constraints, are capable of offering control reserves. Furthermore, the negative dead time (10 s) and the positive dead time (20 s), as well as an amplitude band of 5% of the provided secondary-control power, are specified. The sum of the power values exceeding this band shall not be more than 1% of the area covered by the signal.

At present, the exact regulatory framework for these specifications and requirements provide a basis for judging the ability of aggregated thermostatically controlled appliances and PHEVs to offer secondary control reserves, which will be elaborated in Section V.

III. STUDIED SYSTEM

The system under investigation consists of a network to which the appliances, e.g., PHEVs and thermostatically controlled appliances, are physically connected. In the following, the complete system is described, then the models of the individual units are presented, and a derivation of the aggregated unit models is given.

A. Grid Topology

The investigated system is shown in Fig. 3. It features various energy carriers, here electricity and gas defined in the set \mathcal{E} , and a set of network nodes \mathcal{N} , both given in (2). The system can be understood to model urban agglomerations within a balance group which are supplied by infeeds, found at node 1, from

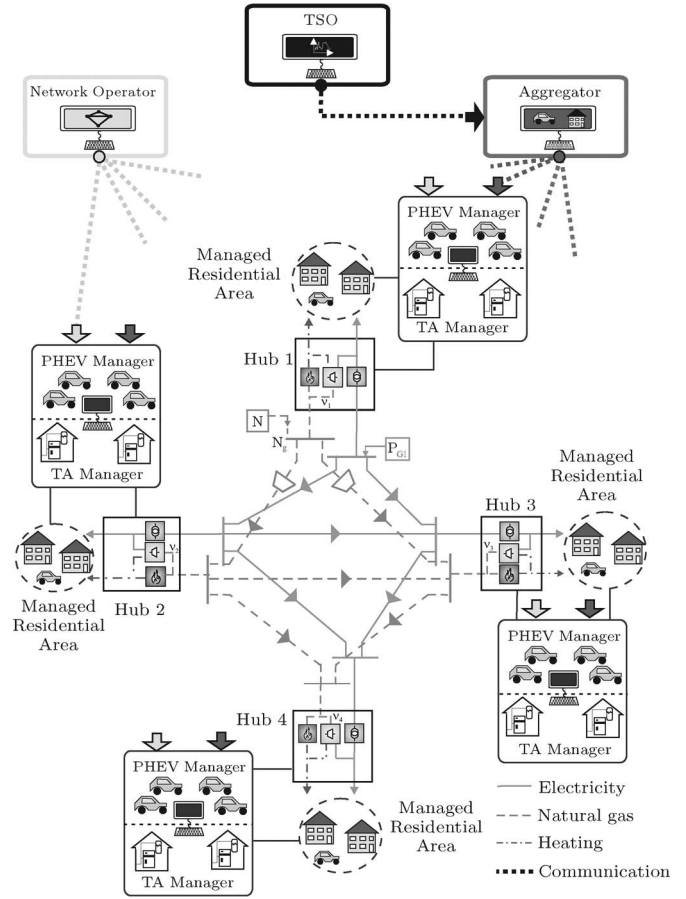


Fig. 3. Four-hub network including PHEV managers for urban areas.

higher voltage levels. Each node is represented by an energy hub [17] included in the set \mathcal{H} . The sets are given as

$$\begin{aligned} e, g, h \in \mathcal{E} &= \{\text{electricity, natural gas, heat}\} \\ m, n, \dots \in \mathcal{N} &= \{1, 2, \dots, N_N\} \\ i, j, \dots \in \mathcal{H} &= \{1, 2, \dots, N_H\}. \end{aligned} \quad (2)$$

The hub performs the conversion of the input-energy carriers in order to supply the respective loads of the area. Here, electricity and natural gas are converted to supply electricity on a lower voltage level and heat. Since electric power can be produced by using natural gas through CHP turbines, the electricity and gas networks are linked (see [17] for a general discussion of interconnected multienergy carrier networks).

Equation (3) specifies the hubs, which include a transformer, a CHP, and a furnace. Their input powers are given by vector \mathbf{P} , their output by vector \mathbf{L} , and the time step by t . The variable ν denotes the dispatch factor, where $\nu + \nu' = 1$. This factor is used to determine the fraction of natural gas flowing into the CHP and the furnace, respectively. The factors in the matrix \mathbf{C} represent the converter efficiencies. The transformer efficiency is given by $\eta_{TR,ee}$, while $\eta_{CHP,ge}$ and $\eta_{CHP,gh}$ are used for the CHP, and $\eta_{F,gh}$ is used for the furnace

$$\underbrace{\begin{bmatrix} L_e(t) \\ L_h(t) \end{bmatrix}}_{\mathbf{L}} = \underbrace{\begin{bmatrix} \eta_{TR,ee} & \nu_g(t)\eta_{CHP,ge} \\ 0 & \nu_g(t)\eta_{CHP,gh} + (\nu'_g(t))\eta_{F,gh} \end{bmatrix}}_{\mathbf{C}} \underbrace{\begin{bmatrix} P_e(t) \\ P_g(t) \end{bmatrix}}_{\mathbf{P}}. \quad (3)$$

The electricity network is modeled by the well-known ac power-flow approach with complex voltages and line impedances. It can be found in [18] and, for multienergy carriers, in [17]. The resistance-to-reactance ratio of the electricity lines is chosen to be one, which is typical for distribution lines.

Gas networks can be modeled similarly using gas nodal balance (4) and line (5) and (6). In (4), $F_{mg}(t)$ gives the gas volume flow injected at node m . Flows between nodes are expressed as functions of the upstream and downstream pressures $p_m(t)$ and $p_n(t)$. The properties of the pipeline and the fluid are represented by the constant k_{mn} [19]. The flow equations are formulated as

$$F_{mg}(t) - \sum_{n \in \mathcal{N}/\{m\}} F_{mng}(t) = 0 \quad (4)$$

$$\forall m \in \mathcal{N} = \{1, 2, \dots, N_N\}$$

$$F_{mng}(t) = k_{mn} s_{mn}(t) \sqrt{s_{mn}(t) (p_m^2(t) - p_n^2(t))} \quad (5)$$

where

$$s_{mn}(t) = \begin{cases} +1, & \text{if } p_m(t) \geq p_n(t) \\ -1, & \text{else.} \end{cases} \quad (6)$$

The power F_{com} consumed by the gas compressors, found in Fig. 3, depends on the applied pressure as well as the volume flow rate and is approximated with

$$F_{\text{com}}(t) = k_{\text{com}} F_{mng}(t) (p_m(t) - p_k(t)) \quad (7)$$

where k_{com} is a constant characterizing the compressor unit and $p_k(t)$ and $p_m(t)$ are the suction and discharge pressures, respectively [17]. The gas power flow $P_{mng}(t)$ between nodes m and n corresponds to the volume rate $F_{mng}(t)$ multiplied by the gross-heating value of the fluid.

The power flow through the system is calculated via the optimization problem denoted in (8)–(10), introduced in [20], where (8) gives the objective function expressing total energy costs. Equation (9a) gives the equality constraints for the hub consumptions. The nodal balances are denoted by \mathbf{G}_α and included through (9b). The curves shown in Fig. 4 display the aggregated electricity load and the aggregated heat load imposed on the system. Equation (10) gives the inequality constraints for the hub power inputs $\mathbf{P}_i(t)$ in (10a), the converter inputs $\mathbf{P}_{ci}(t)$ in (10b), the line flows $\mathbf{F}_\alpha(t)$ in (10c), where α stands for the energy carrier, and the dispatch factors $\mathbf{N}_i(t)$ in (10d) of time step t . The optimization is minimizing

$$f(P_{ei}(t), P_{gi}(t)) = \sum_{i \in \mathcal{H}} \pi_e(t) P_{ei}(t) + \pi_g(t) P_{gi}(t) \quad (8)$$

subject to

$$\mathbf{L}_i(t) - \mathbf{C}_i \mathbf{P}_i(t) = \mathbf{0} \quad \forall i \in \mathcal{H} \quad (9a)$$

$$\mathbf{G}_\alpha(t) (\mathbf{P}_i(t)) = \mathbf{0} \quad \forall \alpha \in \mathcal{E} \quad (9b)$$

$$\underline{\mathbf{P}}_i \leq \mathbf{P}_i(t) \leq \overline{\mathbf{P}}_i \quad \forall i \in \mathcal{H} \quad (10a)$$

$$\underline{\mathbf{P}}_{ci} \leq \mathbf{N}_i(t) \mathbf{P}_i(t) \leq \overline{\mathbf{P}}_{ci} \quad \forall i \in \mathcal{H} \quad (10b)$$

$$\underline{\mathbf{F}}_\alpha \leq \mathbf{F}_\alpha(t) \leq \overline{\mathbf{F}}_\alpha \quad \forall \alpha \in \mathcal{E} \quad (10c)$$

$$\mathbf{0} \leq \mathbf{N}_i(t) \leq \mathbf{1} \quad \forall i \in \mathcal{H}. \quad (10d)$$

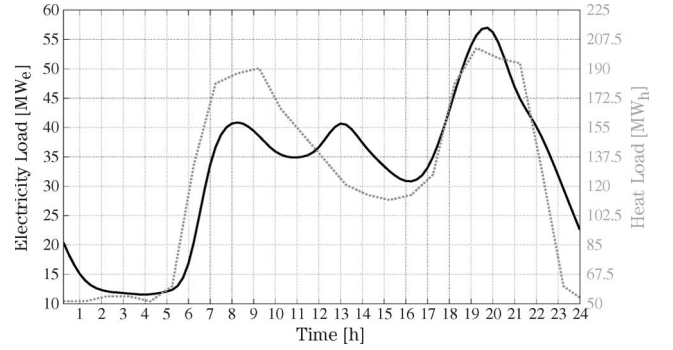


Fig. 4. Electricity and heat load of the system.

B. Unit Locations and Behavior

Each node in the system shown in Fig. 3 includes an intelligent management device in order to control the connected loads. The management devices are presumed to control the PHEVs and the thermostatically controlled appliances in the households at the same time and are referred to as the PHEV manager and thermal appliance (TA) manager.

The PHEV behavior is simulated through an agent-based transportation model [21], [22]. It includes actual PHEV energy consumption, which is calculated through the model described in [23], using real-world drive cycles. The vehicles' daily behavior comprises the activities of *working*, *education*, and *home* [24], which are mapped to a transportation network of almost 28 000 streets. Streets, i.e., activity locations, are contiguously assigned to the network nodes according to their respective geographical information system coordinates, and each street offers different activity possibilities. Pervasive connection points for recharging are assumed, which allow PHEVs to connect throughout the day at every location approached. According to the individual activity plans, PHEVs move within the area supplied by a node, or they may even switch nodes. The agents in the underlying transportation network are shown in Fig. 3 through the light-gray dots.

When the cars are connected, information is sent to the PHEV manager at the specific node. The information includes arrival time, designated departure time, SOC at arrival, desired SOC at departure, battery size, connection power rating, and the information for which mode they can be used. The local PHEV manager considers different possible modes envisioned for PHEVs. The modes include controlled recharging and V2G services. According to the mode information, the PHEV manager inserts the PHEVs into the proper management scheme. An overview of available modes and possible mode transfers is shown in Fig. 5(a) [25].

The V2G mode incorporates the vehicle states of charging, idle, and discharging. Further, it is presumed that PHEVs are able to leave the V2G mode and transfer to controlled recharging when they need to start charging immediately to achieve the desired SOC at departure. In this case, they are not available anymore for LFC through the aggregator. Controlled recharging includes control signals for PHEV demand management, which are based on energy prices but include locational information, e.g., congestion of the network node, as well.

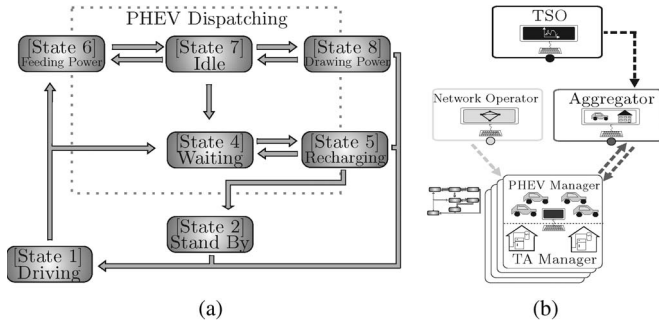


Fig. 5. PHEV operation states and the hierarchical information flow. The PHEV operation states are used by the PHEV manager device at the lowest level. (a) PHEV dispatched between vehicle operation states in the power system. Dispatch is dependent on PHEV objectives [25]. (b) Hierarchical information flow between network entities.

The PHEV management scheme incorporates individual PHEV parameters and has been discussed in [20] and [26]. The wide-scale application of the PHEV manager concept, including a predictive hierarchical approach in a realistic large network, is shown in [27]. The PHEV manager approach comprises the states of waiting (state 4) and charging (state 5) and ensures that the physical constraints of the network are not violated. The controlled recharging mode is presumed to have a higher priority than the V2G mode. This means that the controllable PHEV load is added to the forecasted base load of the respective node, leaving only a certain security margin for LFC (e.g., V2G) services at each node.

The thermostatically controlled appliances are located in the individual households and are owned by the final customers. In the present setup, they are assumed to be capable of “on/off” switching actions, which can be caused by their own hysteresis controller, as well as an external command from the outside. The enforced switching actions serve to influence the current active-power demand of the group of connected appliances. A recently developed duty-cycle coordination scheme [28] provides the possibility to distribute compulsory switching actions onto the group in a structured way. These switching actions can also be computed based on a stochastic representation of the appliance population, as shown in [29]. Another control possibility for set-point tracking, achieving similar results in the aggregation, consists of moving the entire temperature dead band up and down [30].

A basic requirement fulfilled by the coordination algorithm used here is that the permissible temperature range of the appliances is not to be exceeded, and the additional switching actions are minimized in each time step of the switching algorithm. The group under the coordination regime can be characterized by aggregated properties, as shown in [28] and [31], although the individual appliance parameters can be highly diverse. This will be exploited by the Model Predictive Control (MPC) strategy presented in Section IV.

C. Information-Exchange Architecture

The information exchange between the TSO, the aggregator, the Network Operator, and the nodal management devices is structured hierarchically, as shown in Fig. 5(b).

The information flows are shown in Fig. 5(b) via the dashed arrows.

The Network Operator employs the PHEV and TA managers to ensure that the energy system remains in safe operational bounds. For this purpose, the operator performs a load forecast for the controllable thermostatically controlled appliances at their actual steady-state power consumption and the other (noncontrollable) residential load, which is used to calculate the maximal suppliable PHEV load per node. Here, only the transformer-power constraints at the respective nodes are considered.

Subsequently, the maximal suppliable PHEV load per node is sent to the corresponding PHEV manager in order to ensure that no overloading of the system occurs when many PHEVs call for recharging. This maximal allowed PHEV load leaves a security power margin at each transformer. Here, it is chosen such that the household appliances can always be fully activated for control service. The information transmission of the maximal PHEV load is indicated through the light-gray arrow in Fig. 5(b). The PHEV manager uses it to schedule as many PHEVs in controlled recharging mode as possible for recharging without violating the security margin. Finally, the sum of the load of controllable appliances and PHEVs in controlled recharging is used by the Network Operator to calculate the power flow of the multienergy carrier system according to (3)–(10). The steady-state solution gives the available security margins as well as CHP working points.

The aggregator uses the management devices to facilitate the clustering of PHEVs and thermostatically controlled appliances for provision of LFC. The aggregator is also in control of a medium-size CHP unit, which is flexible in its operation and is situated at node 4. The PHEV manager informs the aggregator on the available PHEVs in V2G mode, their SOC, and their individual nodal location, while the TA manager sends information on the individual SOC of the thermostatically controlled appliances. This is indicated via the dashed dark-gray arrow pointing toward the aggregator. The aggregator uses this information together with the LFC signal, received from the TSO, and the available nodal power margins to schedule PHEVs, TAs, and the CHP for LFC. After 15 min (network dispatch time), the PHEV manager takes advantage of the state description of Fig. 5(a) and transfers PHEVs which leave or which immediately need to recharge into the proper mode for the next time step. This is indicated in Fig. 5(b) through the icon to the left of the PHEV manager. PHEVs, which transferred from V2G to the controlled recharging mode, contribute to the loading of the network in the next time step. Then, in case of fully activating the controllable loads at one node together with the maximal PHEV load in controlled recharging mode, no capacity is available at this node for V2G services.

D. Individual Unit Modeling

The modeling of the individual units is presented in the following. The dynamics of the PHEV batteries are easiest to express in discrete time, while the temperature evolution of the

thermostatically controlled appliances and CHP heat storage is better described in continuous time. The variable k denotes the secondary control time step with the step size $\Delta t_{\text{ctrl}} = 10$ s in the present setting as t already represents the dispatch time step, with $\Delta t = 15$ min being the dispatch step size. Whenever a continuous formulation is used, the reference to time is omitted.

1) *PHEVs*: The individual PHEVs can be modeled through a set [(11)] of connected vehicles v at each node n . The set is defined for a time interval t and consists of several subsets (12). These represent the vehicles which are arriving (A), already parked (P), or departing (D) in interval t , which is denoted as

$$v_n \in \mathcal{PHEV}_n(t) = \{1, 2, \dots, N_{\text{PHEV}_n}\} \quad (11)$$

with

$$\mathcal{PHEV}_n(t) = \mathcal{PHEV}_n^A(t) \cup \mathcal{PHEV}_n^P(t) \cup \mathcal{PHEV}_n^D(t). \quad (12)$$

As the dispatch and power flow is carried out once in time step t whereas the tracking of the LFC signal refers to the much shorter time step k , the storage dynamics are formulated with respect to k . The relation between the consumed power $\mathfrak{p}_{\text{PHEV},v_n}(k)$ and the SOC $\mathfrak{e}_{\text{PHEV},v_n}^{\text{rel}}(k)$ (electrical energy contained in the battery relative to the battery capacity) is given by the difference equation

$$\mathfrak{e}_{\text{PHEV},v_n}^{\text{rel}}(k+1) = \mathfrak{e}_{\text{PHEV},v_n}^{\text{rel}}(k) + \eta_{\text{PHEV},\text{eff}} \frac{\Delta t_{\text{ctrl}}}{C_{v_n}^B} \mathfrak{p}_{\text{PHEV},v_n}^{\text{rel}}(k) \quad (13)$$

with the initial condition $\mathfrak{e}_{0,\text{PHEV},v_n}^{\text{rel}} = \mathfrak{e}_{\text{PHEV},v_n}^{\text{rel}}(k = k_0)$. Here, $\eta_{\text{PHEV},\text{eff}}$ is the effective charging/discharging efficiency of the battery, which is equal to $\eta_{\text{PHEV},\text{ch}} = 0.8$ for $\mathfrak{p} > 0$ and is equal to $1/\eta_{\text{PHEV},\text{dc}} = 1.1$ for $\mathfrak{p} < 0$. The SOC is confined to a time-invariant battery-specific range, e.g., [20%, 100%], by the constraint

$$0 \leq \mathfrak{e}_{\text{PHEV},v_n}^{\text{rel}} \leq \mathfrak{e}_{\text{PHEV},v_n}^{\text{rel}}(k) \leq \bar{\mathfrak{e}}_{\text{PHEV},v_n}^{\text{rel}} \leq 1. \quad (14)$$

When determining the available V2G charging and discharging power at a certain point in time, only the vehicles connected at that time can be taken into account. The dispatch step size Δt is used since a time-varying power constraint sampled with the control time step size Δt_{ctrl} appears to be excessive. As it is possible that cars arrive within a certain time interval t , they obviously are not connected for the whole duration of this time step. As a simplification for the controlled recharging mode, their power connection is scaled down, and the cars are assumed to be connected throughout the complete time interval but with a lower power rating. The rating is derived such that the charged energy during the complete interval is equal to the actual charged energy. The respective power connection $\bar{\mathfrak{p}}_{\text{PHEV},v_n}(t)$ (upper constraint of power that a car can draw from the grid) is represented by (15), where $C_{v_n}^P$ is the connection power of PHEV v at node n , Δt is the dispatch interval time length in seconds, and $T_{v_n}^A, T_{v_n}^D$ are arrival and departure time in seconds, respectively. In case the total chargeable energy during one interval exceeds the amount to fully charge/discharge the

vehicle, the maximal power is derived from the SOC via (*) and (**) of

$$\begin{aligned} \bar{\mathfrak{p}}_{\text{PHEV},v_n}^P(t) &= C_{v_n}^P \quad \forall v_n \in \mathcal{PHEV}_n^P(t) \\ \bar{\mathfrak{p}}_{\text{PHEV},v_n}^D(t) &= C_{v_n}^P \frac{T_{v_n}^D - (t-1)\Delta t}{\Delta t} \quad \forall v_n \in \mathcal{PHEV}_n^D(t) \\ \bar{\mathfrak{p}}_{\text{PHEV},v_n}^A(t) &= C_{v_n}^P \frac{(t)\Delta t - T_{v_n}^A}{\Delta t} \quad \forall v_n \in \mathcal{PHEV}_n^A(t) \\ \bar{\mathfrak{p}}_{\text{PHEV},v_n}^{A,D}(t) &= C_{v_n}^P \frac{T_{v_n}^A - T_{v_n}^D}{\Delta t} \quad \forall v_n \in \mathcal{PHEV}_n^{A \cup D}(t) \\ \bar{\mathfrak{p}}_{\text{PHEV},v_n}^1(t) &= \frac{(\bar{\mathfrak{e}}_{v_n}^{\text{rel}} - \mathfrak{e}_{v_n}^{\text{rel}}(t)) C_{v_n}^B}{\Delta t} \quad \forall v_n \in \mathcal{PHEV}_n(t), (*) \\ \bar{\mathfrak{p}}_{\text{PHEV},v_n}^2(t) &= \frac{(\mathfrak{e}_{v_n}^{\text{rel}}(t) - \underline{\mathfrak{e}}_{v_n}^{\text{rel}}) C_{v_n}^B}{\Delta t} \quad \forall v_n \in \mathcal{PHEV}_n(t), (**). \end{aligned} \quad (15)$$

with $C_{v_n}^B$ being the battery capacity [32].

This approach is also performed for vehicles in V2G mode. However, in V2G, the vehicles may feed power back into the grid, which temporarily makes them appear like a generation unit. For consistency of the problem formulation, the cars are modeled as a load which can have a negative power consumption. Thus, the lower power consumption constraint $\underline{\mathfrak{p}}_{v_n}(t)$ is described by

$$\begin{aligned} \underline{\mathfrak{p}}_{\text{V2G},v_n}^{\aleph}(t) &= -\bar{\mathfrak{p}}_{\text{V2G},v_n}^{\aleph}(t) \\ &= -\bar{\mathfrak{p}}_{\text{PHEV},v_n}^{\aleph}(t) \text{ with } \aleph \in \{A, D, P, 1, 2\}. \end{aligned} \quad (16)$$

In order to calculate the available power for a controlled infeed ($\underline{\mathfrak{p}}_{\text{V2G},v_n}(t)$) or consumption ($\bar{\mathfrak{p}}_{\text{V2G},v_n}(t)$) of power in the V2G mode

$$\begin{aligned} \bar{\mathfrak{p}}_{\text{V2G},v_n}(t) &= \min \left\{ \bar{\mathfrak{p}}_{\text{V2G},v_n}^{\aleph}(t), \bar{\mathfrak{p}}_{\text{V2G},v_n}^1(t) \right\} \\ \underline{\mathfrak{p}}_{\text{V2G},v_n}(t) &= \max \left\{ \underline{\mathfrak{p}}_{\text{V2G},v_n}^{\aleph}(t), \underline{\mathfrak{p}}_{\text{V2G},v_n}^2(t) \right\} \\ &\text{with } \aleph \in \{A, D, P\} \end{aligned} \quad (17)$$

is used.

This consideration is necessary to accurately represent the limit in available power from vehicles that are close to their storage limit, as well as vehicles that are not present during the entire time interval t . In case the PHEVs transfer to the controlled recharging mode, (15) is used to calculate the charging power.

However, this introduces an error for LFC capacity calculations as the control step size is much smaller than the period t . Therefore, as a conservative approximation, only the parked vehicles in period t [corresponding to $\aleph \in \{P\}$ in (17)] are used for calculating the available V2G power. The difference between the conservative approach and the other is shown in Fig. 6. There is no discrepancy during the times when all PHEVs are parked. However, during time intervals when many cars depart or arrive, the difference for available power of PHEVs in positive (loading) and negative (feeding)

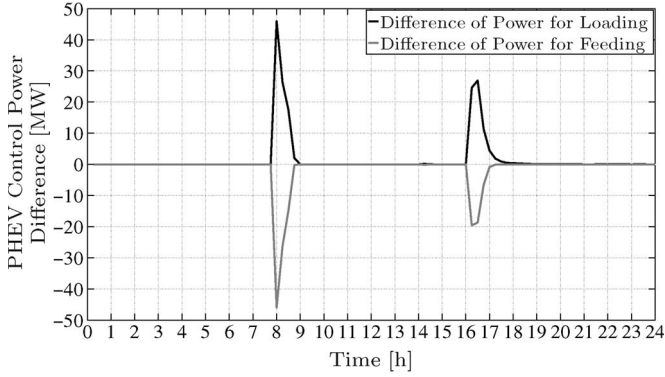


Fig. 6. Difference between optimistic (15) and conservative calculation of controllable power from PHEVs in V2G mode for LFC.

direction is substantial. Note that the maximal LFC capacity provided by PHEVs over the day is 110 MW, as will be shown later.

2) *Controllable Loads*: The group of thermostatically controlled appliances consists of cooling appliances r and heating appliances s at the different nodes n given through sets

$$r_n \in \mathcal{C}_{\text{cool},n} = \{1, 2, \dots, N_{\text{CL,cool},n}\} \quad (18)$$

$$s_n \in \mathcal{C}_{\text{heat},n} = \{1, 2, \dots, N_{\text{CL,heat},n}\}. \quad (19)$$

For brevity, the model is only formulated for a cooling appliance r at node n . As discussed in [33], a TA can be represented by a continuous first-order differential equation describing the temperature evolution between the switching boundaries of the internal thermostat controller as

$$\frac{d\epsilon_{\text{CL},r_n}^{\text{rel}}}{dt} = -\frac{1}{\tau_{\text{CL},r_n}} (\epsilon_{\text{CL},r_n}^{\text{rel}} - \epsilon_{\text{CL,amb},r_n}^{\text{rel}}) + \frac{k_{\text{CL},r_n} u_{r_n}}{\tau_{\text{CL},r_n}} \quad (20)$$

where the thermal time constant τ_{CL,r_n} [s], the amplification factor k_{CL,r_n} [-], and the initial condition $\epsilon_{0,\text{CL},r_n}^{\text{rel}}$ of the differential equation are determined by

$$\tau_{\text{CL},r_n} = \frac{m_{r_n} \bar{c}_{r_n}}{A_{r_n} \bar{\alpha}_{r_n}} \quad (21)$$

$$k_{\text{CL},r_n} = \frac{\epsilon_{\text{th},r_n} p_{\text{CL},r_n}^{\text{rated}}}{A_{r_n} \bar{\alpha}_{r_n} (T_{\text{max},r_n} - T_{\text{min},r_n})} \quad (22)$$

$$\epsilon_{0,\text{CL},r_n}^{\text{rel}} = \epsilon_{\text{CL},r_n}^{\text{rel}}(t = t_0) \quad (23)$$

with the average heat-transfer coefficient $\bar{\alpha}_{r_n}$ [W/(m² · K)], the hull surface A_{r_n} [m²], the average specific-heat capacity \bar{c}_{r_n} [J/(kg · K)], and the mass m_{r_n} [kg] are contained in the appliance. In cooling appliances, the coefficient of performance of the cooling aggregate (including the efficiency of the compressor) is represented by ϵ_{th,r_n} . In water heaters, the efficiency of the heating element is denoted by ϵ_{th,s_n} . Further, $p_{\text{el},r_n}^{\text{rated}}$ [W] is the rated power consumption of the appliance and $T_{\text{max},r_n}, T_{\text{min},r_n}$ (both in [°C]) represent the switching boundaries of the appliance thermostat.

The input u_{r_n} represents a hysteresis switching controller acting according to the temperature boundaries of the appliance as

$$u_{r_n} = \begin{cases} 1, & \text{if } \epsilon_{\text{CL},r_n}^{\text{rel}} \leq 0 \\ 0, & \text{if } \epsilon_{\text{CL},r_n}^{\text{rel}} \geq 1. \end{cases} \quad (24)$$

The net storable electrical energy between the temperature bounds of the appliance can be described by

$$\epsilon_{\text{CL},r_n}^{\text{net}} = \frac{\tau_{\text{CL},r_n}}{k_{\text{CL},r_n}} p_{\text{CL},r_n}^{\text{rated}}. \quad (25)$$

3) *CHP Unit*: The CHP unit at node 4 in the system is available for LFC, and it supplies electricity and heat if used. Its operating point is determined by the optimal power-flow calculation in Section III. Around this operating point, a control band is reserved in which the unit can adapt its power generation in order to participate in the LFC scheme. A heat storage attached to the CHP unit compensates for any heat excess arising from following the control signal. The storage should be operated around an SOC of 50% in the base case in order to allow for control actions in both directions. It is not included in the general system-optimization scheme described earlier as it only acts as a short-term balancing buffer for CHP control services.

This CHP is characterized by power-production constraints and ramp-rate constraints, as well as the heat-storage capacity of the buffer and the governing equation for the temperature dynamics. As the heat storage is assumed to be a water tank with an imperfect insulation, the dynamic model closely resembles the used TA model

$$\frac{dE_{\text{CHP}_4}^{\text{rel}}}{dt} = -\frac{1}{\tau_{\text{CHP}_4}} (E_{\text{CHP}_4}^{\text{rel}} - E_{\text{CHP}_4,\text{amb}}^{\text{rel}}) + \frac{k_{\text{CHP}_4}}{\tau_{\text{CHP}_4}} \left(\frac{\eta_{\text{CHP}_4,\text{th}}}{\eta_{\text{CHP}_4,\text{el}}} P_{\text{CHP}_4} - P_{\text{th},d_4} \right) \quad (26)$$

where $E_{\text{CHP}_4}^{\text{rel}}$ refers to the energy contained in the storage attached to the CHP, $E_{\text{CHP}_4,\text{amb}}^{\text{rel}}$ gives the ambient temperature of the CHP heat storage, P_{th,d_4} represents the thermal demand at node 4, and P_{CHP_4} denotes the current CHP power input, which is derived through (20) using

$$\tau_{\text{CHP}_4} = \frac{m_{\text{CHP}_4} \bar{c}_{\text{CHP}_4}}{A_{\text{CHP}_4} \bar{\alpha}_{\text{CHP}_4}} \quad (27)$$

$$k_{\text{CHP}_4} = \frac{1}{A_{\text{CHP}_4} \bar{\alpha}_{\text{CHP}_4} (T_{\text{max},\text{CHP}_4} - T_{\text{min},\text{CHP}_4})}. \quad (28)$$

The initial condition and constraints are equal to

$$E_{0,\text{CHP}_4}^{\text{rel}} = E_{\text{CHP}_4}^{\text{rel}}(t = t_0), \quad (29)$$

$$0 \leq E_{\text{CHP}_4}^{\text{rel}} \leq 1 \quad (30)$$

$$0 \leq P_{\text{CHP}_4} \leq P_{\text{CHP}_4}^{\text{rated}}. \quad (31)$$

E. Aggregated Representations

In the following, the aggregated representations for the groups of PHEVs and thermostatically controlled appliances

are derived. These will be used subsequently for the control-problem formulation. The aggregation is performed due to the fact that an individual treatment of all appliances and PHEVs in a centralized optimization appears to be computationally demanding, as discussed in [32]. Therefore, the algorithms found in [32] and [33] are used to encapsulate the behavior of the individual units within the aggregated group, allowing the control algorithm to act on the group without having to consider each individual vehicle or TA.

1) *PHEVs*: The aggregated formulation of the total PHEV storage can easily be derived from (15). In order to calculate the total PHEV power available in time step t for a controlled infeed $\underline{P}_{V2G}(t)$, the individual powers are summed over all PHEVs at all nodes. This is denoted in (32). The same is performed in (33) to achieve the total PHEV power for a controlled consumption $\bar{P}_{V2G}(t)$. Finally, the aggregated SOC for V2G services ($SOC_{V2G}(t)$) is calculated via (34). The constraints on power and energy of the aggregated PHEV storage, which are given to the MPC scheme, are formulated in the following:

$$\underline{P}_{V2G}(t) = \sum_{n=1}^{N_N} \sum_{v=1}^{N_{PHEV_n}} \underline{p}_{V2G,v_n}(t) \quad (32)$$

$$\bar{P}_{V2G}(t) = \sum_{n=1}^{N_N} \sum_{v=1}^{N_{PHEV_n}} \bar{p}_{V2G,v_n}(t) \quad (33)$$

$$E_{V2G}^{rel}(k) = \frac{\sum_{n=1}^{N_N} \sum_{v=1}^{N_{PHEV_n}} e_{V2G,v_n}(k)}{\sum_{n=1}^{N_N} \sum_{v=1}^{N_{PHEV_n}} C_{v_n}^B} \quad (34)$$

$$\underline{P}_{V2G}(t) \leq P_{V2G}(t) \leq \bar{P}_{V2G}(t) \quad (35)$$

$$\underline{E}_{V2G} \leq E_{V2G}^{rel}(t) \leq \bar{E}_{V2G}. \quad (36)$$

The previous representation of the PHEVs is used within the control algorithm of the aggregator. This scheme produces a PHEV control signal determining the charge and discharge behavior of the aggregated PHEV storage. The signal is followed by applying the heuristic denoted in (37). For a controlled consumption, the list of PHEVs in V2G mode is sorted with respect to the value of the product of current SOC $e_{V2G,v_n}^{rel}(k)$ and the respective departure time $T_{v_n}^D$. This scheme favors PHEVs which have a low SOC to be recharged and have little time to departure. In the other case, the PHEV V2G list is sorted with respect to maximal SOC for controlled discharging, which favors PHEVs that have a high SOC to be discharged [32], hence

$$S_c(k) = \begin{cases} < 0, & \text{sort ascending } \{e_{V2G,v_n}^{rel}(k) \cdot T_{v_n}^D\} \\ > 0, & \text{sort descending } \{e_{V2G,v_n}^{rel}(k)\} \end{cases} \quad \forall v_n \in \mathcal{PHEV}_n(t) \wedge \forall n \in \mathcal{N}. \quad (37)$$

2) *Controllable Loads*: The individual TA dynamics were formulated in continuous time as this simplifies the representation of the aggregation procedure. According to [33], the individual controllable appliances can be aggregated to one differential equation describing the dynamic behavior of the

load cluster. Details on the aggregation procedure are omitted here for brevity. The derivation is presented for both appliances r and s , and subscripts are only used where indication is necessary due to differences in formulas. Otherwise, the same considerations hold for both types of devices. The aggregated dynamic behavior can be expressed in terms of aggregated relative energy content

$$E_{CL}^{rel} = \frac{E_{CL}}{\bar{E}_{CL}} \quad (38)$$

where \bar{E}_{CL} is the sum over all net energy contents between the temperature boundaries of the appliances, here exemplarily given for cooling appliances through

$$\bar{E}_{CL,cool} = \sum_{n=1}^{N_N} \sum_{r_n=1}^{N_{CL,cool,n}} e_{CL,r_n}^{net} \cdot e_{CL,r_n}^{rel} \quad (39)$$

yielding a dynamic behavior according to the differential equation

$$\frac{dE_{CL}^{rel}}{dt} = -\frac{1}{\bar{\tau}_{CL}} (E_{CL}^{rel} - E_{CL,amb}^{rel}) + \frac{1}{\bar{E}_{CL}} P_{CL} \quad (40)$$

where $\bar{\tau}_{CL}$ [h] is a time constant describing the loading and unloading behavior of the cluster. The initial condition is written as $E_{CL}^{rel}(t = t_0) = E_{0,CL}^{rel}$. The following two constraints on this dynamical system have already been presented in [31]. The current power consumption is constrained in (41) because of the limited cumulated rated power P_{CL}^{rated} [MW] of the appliances and the fact that the coordination algorithm cannot exploit the full range of this quantity.² The constraint in (42) is imposed on the cluster energy level, which should stay between 10% and 90% of the storage capacity E_{CL}^{max} [MWh] in order to avoid chattering of the appliances around one of their switching boundaries

$$0.2 \cdot P_{CL}^{sch} \leq P_{CL} \leq 1.8 \cdot P_{CL}^{sch}, \quad (41)$$

$$0.1 \leq E_{CL}^{rel} \leq 0.9. \quad (42)$$

F. Operating-Point Selection and Shift to Δ Quantities

When formulating the control problem, it is useful to represent the dynamical system such that all input and state variables are equal to zero in steady state. To this end, a coordinate translation is performed for each unit type. The translation moves the origin to the scheduled value, which is the steady-state working point. Thereafter, the system is represented in Δ quantities describing deviations from the scheduled values

$$\begin{aligned} \Delta P &= P - P^{sch} \\ \Delta E &= E - E^{sch}. \end{aligned} \quad (43)$$

²Note that the permissible control band is chosen symmetrical here because of the symmetrical LFC provisioning. However, the power consumption could be increased theoretically to higher values because the steady-state power consumption is usually much lower than half the rated power of the appliance group.

1) *PHEVs*: According to the aggregated PHEV modeling introduced in Section III-E1, a steady state is reached when $P_{V2G}^{sch} = 0$. For the SOC, the scheduled value of $E_{V2G}^{sch} = 0.6$ is chosen as this represents the middle of the permissible range. Thus

$$\Delta P_{V2G} = P_{V2G} \quad \Delta E_{V2G}^{rel} = E_{V2G}^{rel} - 0.6. \quad (44)$$

2) *Controllable Loads*: Considering that the controllable-load cluster shall have a constant consumption profile in the absence of any control action,³ P_{CL}^{sch} must be a constant value that ensures the maintenance of a certain steady-state cluster energy level E_{CL}^{sch} . As a cluster energy level of 50% of the maximum storage content E_{CL}^{max} implies the least impact on the appliance cluster (see [33]), this value is used to calculate the steady-state power consumption, which yields

$$\Delta P_{CL} = P_{CL} - \frac{1}{\tau} \cdot (0.5 \cdot \bar{E}_{CL} - E_{CL,amb}) \quad (45)$$

$$\Delta E_{CL}^{rel} = E_{CL}^{rel} - 0.5. \quad (46)$$

3) *CHP Unit*: The SOC of the storage attached to the CHP unit is constant when the produced thermal power is equal to the heat demand plus the thermal losses. For a steady-state SOC of 50%, the power and energy in Δ quantities can be derived from (26) and is expressed as

$$\Delta P_{CHP_4} = P_{CHP_4} - \frac{\eta_{CHP_4,el}}{\eta_{CHP_4,th}} \times \left(\frac{0.5 - E_{CHP_4,amb}^{rel}}{k_{CHP_4}} + P_{th,d_4} \right) \quad (47)$$

$$\Delta E_{CHP_4}^{rel} = E_{CHP_4}^{rel} - 0.5. \quad (48)$$

IV. CONTROL-PROBLEM FORMULATION

The aggregator's mode of operation for providing LFC within the hierarchical control scheme is shown in Fig. 7. The information on the individual PHEVs in V2G mode is used by the aggregator to construct the aggregated representations in the form of (32)–(36), as well as the priority lists used by

³The heating and cooling appliances installed in private households are usually subject to user-induced disturbances, such as door openings of refrigerators or hot-water draws from a water heater. These disturbances have characteristic relatively predictable profiles during the day and impact the aggregate energy dissipation from the appliances over time. Note that, in the case of water heaters, this holds for ideally mixed water tanks that can be modeled by one average temperature, while a possible thermal stratification would have to be modeled in more detail. If a "tight" set-point tracking control is imposed, two possibilities exist: 1) The power consumption set point is set to a constant scheduled value, leading to an additional fluctuation of the cluster SOC even in the absence of external control actions, or 2) the power consumption set point is scheduled to a nonconstant baseline trajectory, leading to an approximately constant cluster SOC in the absence of external control actions. In both cases, user-induced disturbances are not likely to be prohibitive factors for the proposed LFC scheme, provided that the additional energy dissipation can be detected by the control algorithm through the feedback of state information from the appliances. For simplicity, the user interactions are neglected here and will be subject to future research.

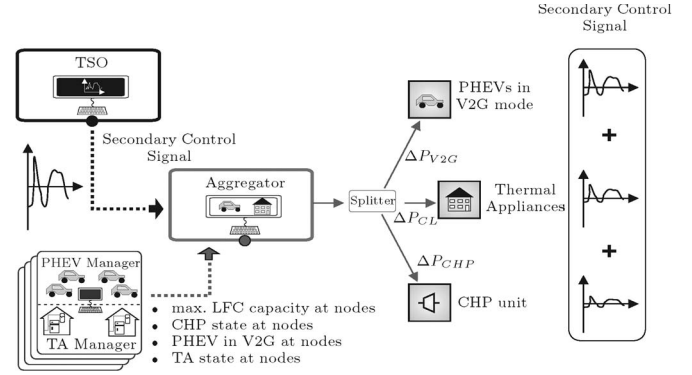


Fig. 7. Provision of LFC through the aggregator within the hierarchical system. The aggregator splits the LFC service between PHEVs in V2G mode, controllable loads, and the CHP.

the heuristic denoted in (37). The signals from the TA managers are used to derive the aggregated representations of the thermostatically controlled appliances according to (38)–(42). The aggregator obtains also information regarding the CHP and solves a control problem, described in the subsequent sections, in order to follow the LFC signal sent by the TSO. The solution provides set points for the aggregated PHEVs, the thermostatically controlled appliances, and the CHP. Hence, the control service request is split between these appliances.

The thermostatically controlled appliances are assumed to be proportionally distributed over the nodes according to the number of served households. The PHEVs, on the other hand, are scheduled depending on the aggregated transformer-power margin and the results of the heuristic. This is based on the assumption that there is no major imbalance of the PHEV number in V2G mode between the nodes, i.e., either the aggregated transformer-power margin is constraining the LFC service of the PHEVs or the number of actually connected PHEVs. Furthermore, if one node should be fully loaded, the PHEVs, which are apparent at this particular node, remain unscheduled and are skipped within the V2G priority lists.

A. Dynamical System

The aggregated representations of controllable loads, PHEVs, and CHP units are combined in one decoupled multiple-input–multiple-output dynamical system for the control-problem formulation. Because of the vast differences in storable energy and time constants, the cooling and refrigeration devices are treated separately from the water heaters. The system of controllable loads and the CHP is formulated in discrete standard notation as

$$\begin{aligned} x(k+1) &= A_d x(k) + B_d u(k) \\ y(k) &= x(k). \end{aligned} \quad (49)$$

The initial condition is $x_0 = x(k = k_0)$, and the state and input variables are defined as

$$x = [\Delta E_{V2G}^{rel}, \Delta E_{CL,cool}^{rel}, \Delta E_{CL,heat}^{rel}, \Delta E_{CHP_4}^{rel}]^T \quad (50)$$

$$u = [\Delta P_{V2G}, \Delta P_{CL,cool}, \Delta P_{CL,heat}, \Delta P_{CHP_4}]^T. \quad (51)$$

The system matrices are diagonal because of the decoupled nature of the dynamics. For expressing the matrices in compact notation, the ‘‘diag’’ operator is used on a column vector, which describes the main diagonal⁴

$$A_d = \text{diag} \begin{bmatrix} \exp\left(-\frac{1}{\bar{\tau}_{CL,cool}} \Delta t_{ctrl}\right) \\ \exp\left(-\frac{1}{\bar{\tau}_{CL,heat}} \Delta t_{ctrl}\right) \\ \exp\left(-\frac{1}{\tau_{CHP_4}} \Delta t_{ctrl}\right) \end{bmatrix} \quad (52)$$

$$B_d = \text{diag} \begin{bmatrix} \frac{1}{E_{V2G}^{max}} \Delta t_{ctrl} \\ -\bar{\tau}_{CL,cool} \frac{\exp(-\Delta t_{ctrl}/\bar{\tau}_{CL,cool})-1}{E_{CL,cool}^{max}} \\ -\bar{\tau}_{CL,heat} \frac{\exp(-\Delta t_{ctrl}/\bar{\tau}_{CL,heat})-1}{E_{CL,heat}^{max}} \\ -\tau_{CHP_4} \frac{\exp(-\Delta t_{ctrl}/\tau_{CHP_4})-1}{E_{CHP_4}^{max}} \end{bmatrix} \cdot \quad (53)$$

B. Penalization Strategy

Some degrees of freedom exist in the construction of the cost function for the MPC strategy. Unlike in classical MPC controllers where the controlled variables shall be brought to the desired value at minimal cost by acting on the control inputs, the rationale behind the present controller is somewhat different. The main task of the controller is to decide which input variable shall be actuated in order to cause the least possible impact on the secondary control signal on the system while following the LFC set point ΔP_{ctrl} , which is sent by the TSO to the aggregator. An exact set-point tracking requires that

$$\begin{aligned} \Delta P_{ctrl}(k) &= \Delta P_{CHP_4}(k) - \Delta P_{CL,heat}(k) - \Delta P_{CL,cool}(k) \\ &\quad - \Delta P_{V2G}(k) \\ &= u_4(k) - u_3(k) - u_2(k) - u_1(k). \end{aligned} \quad (54)$$

Depending on the desired control behavior, the states x_1, \dots, x_4 and inputs u_1, \dots, u_4 can be penalized in different ways. Three possibilities considered in this paper are the following.

- 1) Quadratic penalty for the deviation of a state from its steady-state value, i.e., x_i^2 . This penalty is suitable for units in which the SOC should be kept in the neutral position as much as possible.
- 2) Linear penalization for the absolute deviation of an input from its steady-state value, i.e., $|u_i|$. This serves to penalize the consumption or infeed of a unit, e.g., because of associated energy losses.
- 3) Quadratic penalization of the deviation of a consumption or infeed from its value in the previous time step, i.e., $(u_i(k) - u_i(k-1))^2$. This causes a smoother operation of a unit, e.g., a generation unit with associated ramping costs.

⁴The charging and discharging efficiencies of the PHEVs in V2G mode are not included in order to keep the problem linear. Deviations of predicted and aggregated SOC are accounted for in updating the model state within the receding-horizon control strategy.

The selection of the penalization strategy for the units is based on the following.

- 1) The PHEVs possess a limited storage efficiency and large storage capacity compared with their power rating. This implies that consumptions and infeeds have a rather small effect on the aggregated SOC but cause energy losses, which calls for penalization according to 2).
- 2) For both heating and cooling loads, changes in power consumption have little effect, while the aggregated SOC should be kept as close as possible to the steady state. This is reflected in the choice of penalization strategy 1).
- 3) In the case of CHP units, both a neutral position of the heat storage and a smooth operation is beneficial, which makes it suitable for strategies 1) and 3).

A further aspect to be considered is the effect of the different penalty terms on the conditioning of the optimization problem. Careful tuning has to be applied in order to prevent convergence problems, e.g., due to a very small cost-function gradient.

C. Cost Function and Constraints

Taking into account the penalization rationale developed in the previous section, the cost function can be formulated as a summation of the individual terms to be penalized from a time step k up to a prediction horizon N

$$\begin{aligned} J(k) &= \sum_{l=k}^{k+N-1} x^T(l) Q x(l) + \sum_{l=k}^{k+N-1} \delta u^T(l) R \delta u(l) \\ &\quad + \sum_{l=k}^{k+N-1} \sum_{i=1}^4 R_{abs,i} |u_i(l)| \end{aligned} \quad (55)$$

with $\delta u(l) = u(l) - u(l-1)$. This problem formulation can be implemented easily using MPC environments such as YALMIP [34]. In the case of manual construction of the Hessian matrix and the gradient vector of a quadratic problem in standard notation, the absolute $|\cdot|$ should be dealt with by using auxiliary variables.

The problem is subject to the constraints that have been presented before in Sections III-D and E

$$x(l+1) = A_d x(l) + B_d u(l) \quad (56)$$

$$-0.4 \leq x_{1,2,3}(l) \leq 0.4 \quad (57)$$

$$-0.5 \leq x_4(l) \leq 0.5 \quad (58)$$

$$\Delta P_{V2G}(t) \leq u_1(l) \leq \Delta \bar{P}_{V2G}(t) \quad (59)$$

$$-0.8 \cdot P_{CL,cool}^{sch} \leq u_2(l) \leq 0.8 \cdot P_{CL,cool}^{sch} \quad (60)$$

$$-0.8 \cdot P_{CL,heat}^{sch} \leq u_3(l) \leq 0.8 \cdot P_{CL,heat}^{sch} \quad (61)$$

$$\Delta P_{CHP_4} \leq u_4(l) \leq \Delta \bar{P}_{CHP_4} \quad (62)$$

$$\delta P_{CHP_4} \leq \delta u_4(l) \leq \delta \bar{P}_{CHP_4} \quad (63)$$

$$\Delta P_{ctrl}(k) = u_4(k) - u_3(k) - u_2(k) - u_1(k) \quad (64)$$

$$\Delta P_{ctrl}(t) \leq \Delta P_{ctrl}(k) \leq \bar{P}_{ctrl}(t) \quad (65)$$

TABLE I
SYSTEM PARAMETRIZATION FOR A CASE STUDY

Description	Parameter	Value
City		
Population		160'000
Persons / Household(HH)		2.00
PHEVs / HH		0.5
% Fridges / HH		80 %
% Fridge-Freezers / HH		30 %
% Freezer / HH		60 %
% Water-heaters / HH		30 %
Grid		
Hub 1 trafo power	$P_{TR_1}^{rated}$	30 MW
Hub 2 trafo power	$P_{TR_2}^{rated}$	30 MW
Hub 3 trafo power	$P_{TR_3}^{rated}$	30 MW
Hub 4 trafo power	$P_{TR_4}^{rated}$	30 MW
Transformer efficiency	$\eta_{TR,e e}$	0.98
Furnace efficiency	$\eta_{F,g h}$	0.75
PHEVs		
Total quantity	N_{PHEV}	40'000
Hub 1 quantity	N_{PHEV_1}	10'000
Hub 2 quantity	N_{PHEV_2}	10'000
Hub 3 quantity	N_{PHEV_3}	10'000
Hub 4 quantity	N_{PHEV_4}	10'000
Connection Power	$C_{v_n}^P$	3.5 kW
Battery size	$C_{v_n}^B$	20 kWh
Charging efficiency	$\eta_{PHEV,ch}$	0.8
Discharging efficiency	$\eta_{PHEV,dc}$	0.9
Cooling loads		
Total quantity	$N_{CL,cool}$	136,000
Steady-state consumption	$P_{sch_{CL,cool}}$	6.56 MW
Rated power	$P_{CL,cool}^{rated}$	19.7 MW
Electrical storage capacity	$\bar{E}_{CL,cool}$	1.34 MWh
Rel. ambient energy level	$E_{CL,cool}^{amb}$	-10.84 MWh
Time constant	$\bar{\tau}_{CL,cool}$	1.76 h
Heating loads		
Total quantity	$N_{CL,heat}$	24,000
Steady-state consumption	$P_{sch_{CL,heat}}$	7.38 MW
Rated power	$P_{CL,heat}^{rated}$	72.2 MW
Electrical storage capacity	$\bar{E}_{CL,heat}$	16.07 MWh
Rel. ambient energy level	$E_{CL,heat}^{amb}$	-168.32 MWh
Time constant	$\bar{\tau}_{CL,heat}$	23.88 h
CHP units		
Hub 1 power	$P_{CHP_1}^{rated}$	5 MW
Hub 2 power	$P_{CHP_2}^{rated}$	3 MW
Hub 3 power	$P_{CHP_3}^{rated}$	3 MW
Hub 4 power	$P_{CHP_4}^{rated}$	10 MW
Hub 4 storage	\bar{E}_{CHP_4}	3.48 MWh
Storage time constant	τ_{CHP_4}	145.14 h
Maximum storage temp.	T_{max,CHP_4}	90 °C
Minimum storage temp.	T_{min,CHP_4}	60 °C
Thermal efficiency	$\eta_{CHP_4,th}$	0.55
Electrical efficiency	$\eta_{CHP_4,el}$	0.4
Ramping capability	\dot{P}_{CHP_4}	0.5% / s $P_{CHP_4}^{rated}$
Controller		
Prediction horizon	N	2
State deviation penalty	Q	diag [0 0.25 25 200]
Input move suppression	R	diag [0 0 0 0]
Input absolute penalty	R_{abs}	diag [0.075 0 0 0]
Offered control reserves	ΔP_{ctrl}^{offer}	40 MW

Equation (65) represents an aggregation of the transformer constraints which may prevent the control signal from assuming a desired value. The sizing of the control signal (i.e., the amount of secondary-reserve capacity $\Delta P_{ctrl}^{offer} = \Delta P_{ctrl}/Y$), where Y is the control signal in per unit, must take into account these principal limitations.

Furthermore, it should be noted that one or several of these constraints can be reformulated as soft constraints in order to prevent the problem from becoming infeasible in certain operational situations. As this is relatively straightforward, it is not elaborated in this paper. The unit sizing and scaling of the control signals in the case study presented in Section V is chosen such that infeasibility problems do not occur.

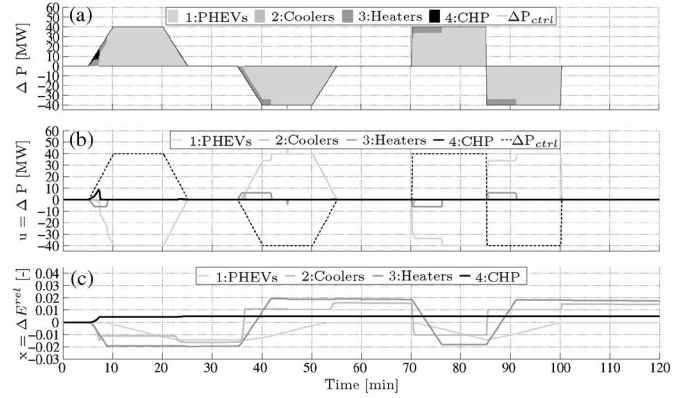


Fig. 8. Tracking of the *swissgrid* prequalification profile. (a) Prequalification signal and contribution from the aggregated appliances in order to follow it. (b) Power deviation from the appliances' steady state. (c) Aggregated state variables.

V. CASE STUDY

In order to demonstrate the presented control approach, numerical time-domain simulations are conducted for two test cases: the tracking of the LFC prequalification profile presented in Fig. 2 and the tracking of a real LFC signal. The numerical values for the system and the parameters of the controller are presented in Table I.

A. Prequalification Profile

Fig. 8 shows the aggregator's response to the prequalification signal and its effect on the aggregated units. In Fig. 8(a), the prequalification signal sent out by the TSO is displayed through the black line confining the stacked area plots. The appliance-group contribution determined by the aggregator is visualized through the stacked plots filling the area under the prequalification signal. It can be seen that the contribution of the PHEVs accounts for a substantial part of the demanded LFC power. This is due to the fact that their response time is short and also that the situation was simulated during nighttime when almost all PHEVs are parked, therefore offering a large controllable power block. The other contributions are provided by the heating appliances, by the CHP, and by the cooling appliances. However, due to their limited storage capacity and the differing penalization factors in the MPC objective function (55) weighing the deviation from the appliances' steady-state energy-storage level, their contributions are smaller. The heaters, and to a minor extent, the CHP, provide power mostly in the beginning of the ramps and steps. The cooling devices barely provide power for LFC. In Fig. 8(a), it can be seen that the prequalification signal is followed.

In Fig. 8(b), the actual set points of the unit are shown. They obviously relate to the prequalification signal and the results shown in Fig. 8(a). The impact of the control variables, i.e., set points, on the appliances' energy content is shown in Fig. 8(c). Note that the heaters exhibit the highest deviation from the steady state. The second highest deviation is found for the coolers. This is due to their comparably lower storage capacity, limiting the provision of LFC, as shown in Fig. 8(a).

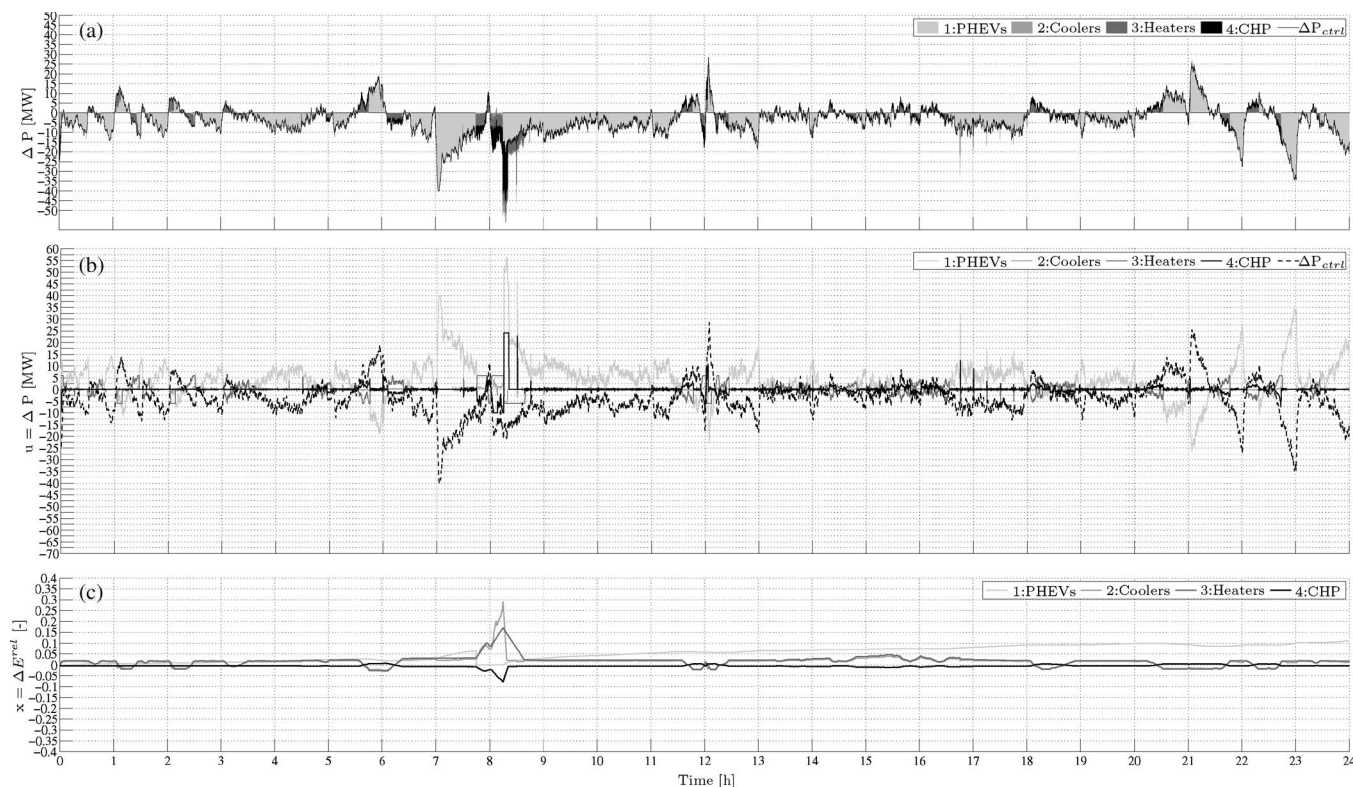


Fig. 9. Tracking a real LFC in the range of ± 40 MW. (a) LFC signal and contributions of the aggregated units. (b) Aggregated input variables. (c) Aggregated state variables.

Only a small contribution from the coolers is found. As the CHP produces excessive power during the first ramp of the pre-qualification signal, the heat storage incurs a positive deviation from its steady state. Although the CHP short-term heat storage includes losses in the current implementation, the storage does not exhibit high losses since the depicted time interval is too short.

B. Tracking of Real LFC Signal

Now, the aggregator is utilized for LFC in the range of up to 40 MW over a full day. The results are shown in Fig. 9. Fig. 9(a), similar to Fig. 8(a), displays the LFC signal sent by the TSO and the contributions of the PHEVs, the household appliances, and the CHP. The LFC signal incorporates frequent oscillations and a negative bias over the day. Such bias poses a challenge for the provision of LFC through storage devices as they might run into overflow or depletion. However, the negative bias is also an advantage because, on average, the PHEV fleet, which is used for LFC, will be recharged. Fig. 9(b) shows the individual controlled power set points sent to the clusters of appliances, while Fig. 9(c) shows the appliances' energy-storage deviation from their steady state.

It can be seen that the highest contribution to LFC is again provided by the PHEVs. The PHEVs are charged, on average, as illustrated in detail by the positive PHEV set points shown in Fig. 9(b). However, although the PHEVs are frequently charged, the overall impact on the cluster in terms of energy deviation remains small, as shown in Fig. 9(c) through the

brightest gray graph. The PHEV cluster barely deviates from its steady-state energy content.

The heating appliances provide the second highest LFC contribution, particularly when the PHEVs are not available. This is the case between 5:00 A.M. and 8:30 A.M. and between 2:00 P.M. and 4:00 P.M., illustrated by the darkest gray graph. The heaters are supported by the cooling appliances, which offer much less available storage, and the CHP. Between 5:00 A.M. and 8:30 A.M., the heaters, the coolers, and the CHP storage exhibit large deviations from their storages' steady-state values. The coolers reach almost 30% deviation from their steady-state energy content, while the heaters reach almost 20%. A large portion of the control power is provided by the CHP, which is regulated down from its current operation point. However, as soon as large numbers of PHEVs arrive at their morning destinations, e.g., work, education, etc., the PHEVs draw more power than necessary for supplying the LFC in order to relieve the heaters and the coolers. Also, the CHP is regulated up again in order to recharge its short-term energy storage. This behavior is due to the penalization strategy of the MPC controller. The energy turnover between PHEVs on one hand and the cooler, the heaters, and the CHP on the other occurs because the penalty factors in the steady-state energy deviation are different, and the storages' states, in this case, differ largely. Therefore, the turnover minimizes the appliances' steady-state deviation. The PHEV storage barely deviates from its steady state. This is due to the fact that it offers a large storage potential. In particular, the PHEV fleet possesses enough potential to supply 40 MW of LFC almost over the complete day, except during the traveling hours. At the

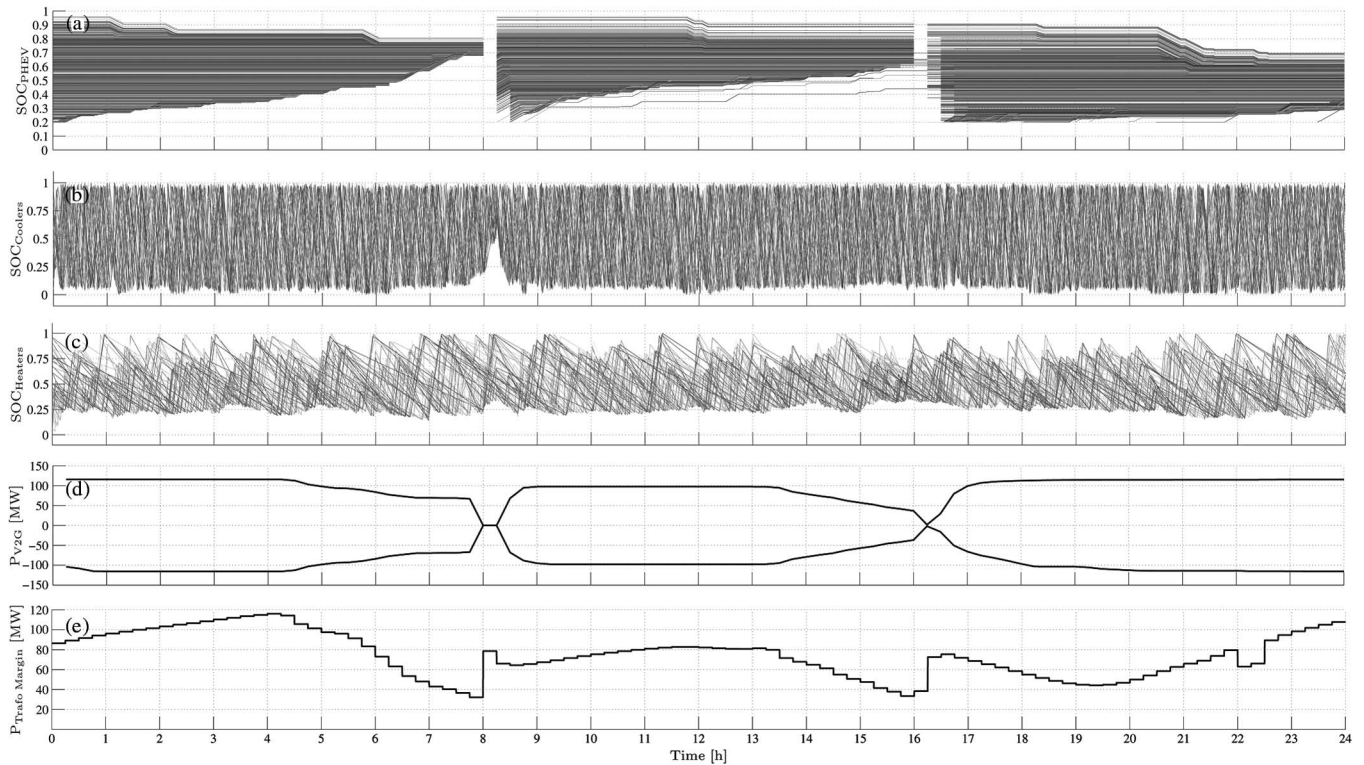


Fig. 10. Impact of LFC on individual appliances in the different clusters. The aggregated V2G power and transformer margins are plotted as well. (a) SOC of selected individual PHEVs in V2G mode. (b) SOC of selected individual cooling appliances. (c) SOC of selected individual heating appliances. (d) Connected overall power of PHEVs in V2G mode. (e) Transformer-power margin left for LFC.

end of the day, only a 10% deviation can be seen for the PHEV cluster, although it was providing most of the LFC services for several hours in the afternoon or night.

Fig. 10 shows the response of the individual appliances in the cluster, the V2G potential, and the useable transformer capacity for LFC throughout the whole day.

In Fig. 10(a), the state variables, i.e., the individual SOC of the PHEVs in V2G mode, are shown. The individual SOC of 1000 randomly sampled PHEVs differ significantly, but each of them stays constant for most of the plotted vehicles. This is due to the fact that the batteries have no standby losses and that the demanded overall energy is relatively small compared with the overall available stored energy. Furthermore, many PHEVs are not scheduled for V2G services because they are on the lower end of the LFC priority lists, as determined by (37). Fig. 10(a) shows also that the heuristic works as desired, and the PHEVs with the highest SOC are discharged and the ones with the lowest are charged. Here, it can be seen again how the negative bias of the LFC signal affects the PHEV fleet. The plot shows that many PHEVs which have a low SOC are able to increase their energy level by providing LFC. During periods where the LFC signal is positive, only the PHEVs are discharged, which incorporate the highest SOC at around 9:00 P.M. The V2G availability is almost zero when many of the PHEVs are either recharging in controlled recharging mode in order to leave soon or have already departed.

The SOC of the cooling and the heating devices is shown in Fig. 10(b) and (c), respectively. Contrary to the stable SOC of the PHEVs, the individual SOC of the household appliances varies since losses are included. Power-consumption set points

forced by the coordination algorithm increase or decrease their SOC. Note that, obviously, all devices stay within their accepted SOC range. The trenches of the band of the enclosing shape are due to the appliances' charging periods when the PHEVs are not available. The household appliances incorporate the advantage to be constantly dispatchable for LFC, since the enclosing shape does not exhibit any continuous separation.

Fig. 10(d) shows the available V2G power potential for LFC throughout the day. Here, the discontinuities of V2G availability are stressed again. Note that during the connection periods, when many PHEVs are in V2G mode, large power capacities between ± 100 MW are potentially available for LFC. However, these decrease rapidly before the PHEVs depart, since they transfer from V2G mode into the controlled recharging mode, where they cannot be scheduled for LFC anymore and just contribute to the loading of the system. Furthermore, it can be seen that, while providing LFC, the available power for these services changes slightly. This is because fully recharged PHEVs discharge due to LFC, which creates some space in their batteries which, vice versa, is then available for recharging, as can be seen around 9:00 P.M. On the other hand, the fully depleted PHEVs are able to recharge their batteries from LFC and are then able to feed power back to the grid, as can be seen between 0:00 A.M. and 1:00 A.M.

Fig. 10(e) shows the available aggregated transformer capacity of the system for the day. It rapidly decreases early in the morning since many PHEVs transfer from the V2G mode into the controlled recharging mode and, hence, add to the noncontrollable load of the system. The residual available aggregated capacity of the transformers is 10.3 MW, which is

the security margin kept for LFC. The margin is ensured at all times by the PHEV managers, which distribute power to large numbers of PHEVs in controlled recharging mode according to the maximal load information transmitted from the Network Operator. The supply of LFC through controllable household appliances is therefore constantly ensured.

VI. DISCUSSION

It was illustrated that LFC can be effectively provided by loads, such as PHEVs and household appliances, within a physical power system in the presence of a suitable communication system, aggregation methods, and control strategies. The aggregation is performed by a supervisory entity called the aggregator, which is using a receding-horizon optimization technique considering physical network constraints and constraints on appliance availability, power, and energy state to provide ancillary services.

Case studies of a large urban agglomeration comprising a population of 160 000 individuals and 40 000 PHEVs illustrated that typical prequalification tests of the TSO can be passed, and 40 MW of LFC for a full day can be offered. A biased LFC signal, varying PHEV availability, and limitations of the underlying physical distribution network were taken into account.

A crucial open question for the practical implementation of the presented scheme is the dimensioning of control reserves offered to the market. As both PHEVs and controllable heating and cooling appliances possess a limited storage capacity, the time-series properties of the control signal, or rather its time integral, are important. This holds both for normal operation as well as for emergency situations, in which a control action might have to be sustained in one direction for a longer time.

Furthermore, the complete power potential available during some periods of the day, e.g., when it would have been possible to offer more than 100 MW, could not be utilized for LFC. The provision of the contracted amount of LFC services must be sustained over long time periods, e.g., depending on the market rules, this could be a whole day. Hence, the maximal amount which can be offered is bounded by the heating and cooling appliances' power capacity and energy storage. In order to take better advantage of the PHEVs' potential for LFC while considering their varying availability, the LFC market process would need to be changed to shorter time intervals. Contracting LFC on an hourly basis or even shorter could allow an aggregator to provide significantly more than 50 MW for LFC. However, in such a case, the underlying physical constraints, such as the power security margins, would need to be revised in order to avoid negative network impacts of LFC.

VII. CONCLUSION

A new power-system entity called aggregator could potentially evolve with the increasing penetration of fast information and communication technology in power systems. Aggregators of large numbers of small controllable loads, such as PHEVs and household appliances, were suggested to contribute to ancillary service provision. This paper has illustrated that aggregated loads can, under certain circumstances like pervasive fast

communication, be effectively used for LFC. Clustering large numbers of PHEVs and household appliances offers substantial amounts of controllable power which can be scheduled without stressing the underlying physical network or violating their individual power and energy constraints.

However, the implementation of such aggregation algorithms and control strategies might introduce computational challenges in the existing setup. One could envision distributed computing to resolve such challenges. Also, more attention needs to be paid to the splitting of the control request among the nodes of a large network in order to maintain a stable network state.

ACKNOWLEDGMENT

The authors would like to thank R. Waraich from IVT, Swiss Federal Institute of Technology (ETH) Zurich, for providing the transportation simulation data.

REFERENCES

- [1] Y. G. Rebours, D. S. Kirschen, M. Trotignon, and S. Rossignol, "A survey of frequency and voltage control ancillary services—Part II: Economic features," *IEEE Trans. Power Syst.*, vol. 22, no. 1, pp. 358–366, Feb. 2007.
- [2] E. O. Lawrence, G. Heffner, C. Goldman, M. Kintner-Meyer, and B. Kirby, *Loads Providing Ancillary Services: Review of International Experience; Technical Appendix: Market Descriptions*, 2007.
- [3] A. Timbus, M. Larsson, and C. Yuen, "Active management of distributed energy resources using standardized communications and modern information technologies," *IEEE Trans. Ind. Electron.*, vol. 56, no. 10, pp. 4029–4037, Oct. 2009.
- [4] A. Hajimiragha, C. Canizares, M. W. Fowler, and A. Elkamel, "Optimal transition to plug-in hybrid electric vehicles in Ontario-Canada considering the electricity grid limitations," *IEEE Trans. Ind. Electron.—Special Issue on Plug-In Hybrid Vehicles*, vol. 57, no. 2, pp. 690–701, Feb. 2010.
- [5] S. M. Lukic, J. Cao, R. C. Bansal, F. Rodriguez, and A. Emadi, "Energy storage systems for automotive applications," *IEEE Trans. Ind. Electron.*, vol. 55, no. 6, pp. 2258–2267, Jun. 2008.
- [6] P. Strauss and M. Braun, "A review on aggregation approaches of controllable distributed energy units in electrical power systems," *Int. J. Distrib. Energy Resour.*, vol. 4, no. 4, pp. 297–319, 2008.
- [7] C. Quinn, D. Zimmerle, and T. H. Bradley, "The effect of communication architecture on the availability, reliability, and economics of plug-in hybrid electric vehicle-to-grid ancillary services," *J. Power Sources*, vol. 195, no. 5, pp. 1500–1509, Mar. 2010.
- [8] W. Kempton and J. Tomic, "Vehicle-to-grid power implementation: From stabilizing the grid to supporting large-scale renewable energy," *J. Power Sources*, vol. 144, no. 1, pp. 280–294, Jun. 2005.
- [9] S. L. Andersson, A. K. Eloffsson, M. D. Galus, L. Göransson, S. Karlsson, F. Johnsson, and G. Andersson, "Plug-in hybrid electric vehicles as regulating power providers: Case studies of Sweden and Germany," *Energy Policy*, vol. 38, no. 6, pp. 2751–2762, Jun. 2010.
- [10] A. Ulbig, M. D. Galus, and G. Andersson, "General frequency control with aggregated control reserve capacity from time-varying sources: The case of PHEVs," in *Proc. IREP Symp.—Bulk Power System Dynamics and Control VIII*, Buzios, Brazil, 2010.
- [11] J. A. Pecos Lopes, P. M. Rocha Almeida, and F. J. Soares, "Using V2G to maximize the integration of intermittent renewable energy resources in islanded electric grids," in *Proc. IEEE ICCEP*, Capri, Italy, 2009, pp. 290–295.
- [12] *Continental Europe (CE) Operation Handbook*, ENTSO-E, 2004. [Online]. Available: <http://www.entsoe.eu>
- [13] Y. G. Rebours, D. S. Kirschen, M. Trotignon, and S. Rossignol, "A survey of frequency and voltage control ancillary services—Part I: Technical features," *IEEE Trans. Power Syst.*, vol. 22, no. 1, pp. 350–357, Feb. 2007.
- [14] C. Maurer, S. Krahl, and H. Weber, "Dimensioning of secondary and tertiary control reserve by probabilistic methods," *Eur. Trans. Elect. Power*, vol. 19, no. 4, pp. 544–552, May 2009.
- [15] swissgrid, *Test for Prequalification of Secondary Control*, 2008.
- [16] swissgrid, *Transmission Code*, 2010.

- [17] M. Geidl and G. Andersson, "Optimal power flow of multiple energy carriers," *IEEE Trans. Power Syst.*, vol. 22, no. 1, pp. 145–155, Feb. 2007.
- [18] J. W. Wood and F. B. Wollenberg, *Power Generation, Operation and Control*, 2nd ed. New York: Wiley-Interscience, 1996.
- [19] E. S. Menon, *Gas Pipeline Hydraulics*. Boca Raton, FL: Taylor & Francis, 2005.
- [20] M. D. Galus and G. Andersson, "Integration of plug-in hybrid electric vehicles into energy systems," in *Proc. IEEE Bucharest Powertech*, Bucharest, Romania, 2009, pp. 1–8.
- [21] M. Balmer, K. Nagel, and B. Raney, "Large-scale multi-agent simulations for transportation applications," *J. Intell. Transp. Syst.: Technol., Plan., Oper.*, vol. 8, no. 4, pp. 205–221, Oct. 2004.
- [22] M. Balmer, K. W. Axhausen, and K. Nagel, "Agent-based demand-modelling framework for large-scale microsimulations," *Transp. Res. Rec.: J. Transp. Res. Board*, vol. 1985, pp. 125–134, 2006.
- [23] M. D. Galus and G. Andersson, "Power system considerations of plug-in hybrid electric vehicles based on a multi energy carrier model," in *Proc. IEEE PES Gen. Meeting*, Calgary, AB, Canada, 2009, pp. 1–8.
- [24] R. Waraich, M. D. Galus, C. Dobler, M. Balmer, G. Andersson, and K. W. Axhausen, "Plug-in hybrid electric vehicles and smart grid: Investigations based on a micro-simulation," in *Proc. Conf. IATBR*, Jaipur, India, 2009.
- [25] M. D. Galus, M. Zima, and G. Andersson, "On integration of plug-in hybrid electric vehicles into existing power system structures," *Energy Policy*, vol. 38, no. 11, pp. 6736–6745, Nov. 2010, DOI: 10.1016/j.enpol.2010.06.043.
- [26] M. D. Galus and G. Andersson, "Demand management for grid connected plug-in hybrid electric vehicles (PHEVs)," in *Proc. IEEE Energy 2030 Conf.*, Atlanta, GA, 2008, pp. 1–8.
- [27] M. D. Galus, R. W. Waraich, and G. Andersson, "Predictive, distributed hierarchical charging control of PHEVs in the distribution system of a large urban area incorporating a multi agent transportation simulation," in *Proc. PSCC*, Stockholm, Sweden, 2011.
- [28] S. Koch, D. Meier, M. Zima, M. Wiederkehr, and G. Andersson, "An active coordination approach for thermal household appliances—Local communication and calculation tasks in the household," in *Proc. IEEE Bucharest PowerTech*, Bucharest, Romania, 2009, pp. 1–8.
- [29] S. Koch, J. Mathieu, and D. Callaway, "Modeling and control of aggregated heterogeneous thermostatically controlled loads for ancillary services," in *Proc. PSCC*, Stockholm, Sweden, 2011, pp. 1–7.
- [30] D. S. Callaway, "Tapping the energy storage potential in electric loads to deliver load following and regulation, with application to wind energy," *Energy Convers. Manage.*, vol. 50, no. 5, pp. 1389–1400, May 2009.
- [31] S. Koch, M. Zima, and G. Andersson, "Potentials and applications of coordinated groups of thermal household appliances for power system control purposes," in *Proc. IEEE PES/IAS Conf. Sustainable Alternative Energy*, Valencia, Spain, 2009, pp. 1–8.
- [32] M. D. Galus, R. La Fauci, and G. Andersson, "Investigating PHEV wind balancing capabilities using heuristics and Model Predictive Control," in *Proc. IEEE PES Gen. Meeting*, Minneapolis, MN, 2010, pp. 1–8.
- [33] S. Koch, M. Zima, and G. Andersson, "Active coordination of thermal household appliances for load management purposes," in *Proc. IFAC Symp. Power Plants Power Syst. Control*, Tampere, Finland, Jul. 2009.
- [34] J. Löfberg, "YALMIP: A toolbox for modeling and optimization in MATLAB," in *Proc. CACSD Conf.*, Taipei, Taiwan, 2004, pp. 284–289.



Matthias D. Galus (S'07) was born in Swientochlowitz, Poland. He received the Dipl.-Ing. degree in electrical engineering and the Dipl.-Ing. degree in industrial engineering from Rheinisch-Westfälische Technische Hochschule (RWTH), Aachen, Germany, in 2005 and in 2007, respectively. He is currently working toward the Ph.D. degree at the Power Systems Laboratory, Swiss Federal Institute of Technology (ETH) Zurich, Zurich, Switzerland, where he joined in 2007.

His research is dedicated to modeling, optimization, and efficient integration of plug-in hybrid electric vehicle into power systems.

Mr. Galus is a member of the German Society of Electrical Engineers (VDE).



Stephan Koch (S'08) was born in Bielefeld, Germany. He received the Dipl.-Ing. degree in engineering cybernetics from the University of Stuttgart, Stuttgart, Germany, in 2007. He is currently working toward the Ph.D. degree at the Power Systems Laboratory, Swiss Federal Institute of Technology (ETH) Zurich, Zurich, Switzerland, where he joined in October 2007.

His work for the project Local Load Management is focused on control and operation strategies for flexible household loads and their technical and economic integration into power systems and electricity markets. His further research interests are automatic control in power systems and system integration of distributed and renewable energy resources.



Göran Andersson (M'86–SM'91–F'97) was born in Malmö, Sweden. He received the M.S. and Ph.D. degrees from the University of Lund, Lund, Sweden, in 1975 and 1980, respectively.

In 1980, he was with the HVDC Division of ASEA, now ABB, Ludvika, Sweden, and in 1986 he was appointed Full Professor in electric power systems with the Royal Institute of Technology (KTH), Stockholm, Sweden. Since 2000, he has been a Full Professor in electric power systems with the Swiss Federal Institute of Technology (ETH), Zurich, Zurich, Switzerland. His research interests are power system analysis, simulation, and control. His other research interest is future energy and power systems.

Dr. Andersson was the recipient of the IEEE Power Engineering Society (PES) Outstanding Power Educator Award 2007. He is a member of the Royal Swedish Academy of Engineering Sciences and Royal Swedish Academy of Sciences, and he is active in IEEE PES.